

Convection in the central Irminger Sea; insights into variability and the roles of surface forcing and stratification from 19 years of high resolution mooring data

M. F. de Jong¹, K. E. Fogaren², I. Le Bras³, L. McRaven³ and H. Palevsky²

¹Royal Netherlands Institute for Sea Research (NIOZ), Department of Ocean Systems, Texel, the Netherlands. ²Boston College, Morrissey College of Arts and Sciences, Chestnut Hill, MA, USA.

³Woods Hole Oceanographic Institution, Woods Hole, MA, USA.

Corresponding author: Femke de Jong (femke.de.jong@nioz.nl)

Key Points:

- Convection in the Irminger Sea has varied between 288 and 1500 dbar in the period from 2002 to 2020, with a mean of 470 dbar.
- Convection since the winter of 2014-2015 have cooled and freshened the central Irminger Sea, although this event was not as strong as in the 1990s
- Atmospheric forcing is three times as important as stratification in determining the maximum mixed layer depth

Abstract

Transformation of light to dense waters by atmospheric cooling is key to the Atlantic Meridional Overturning in the Subpolar Gyre. Convection in the center of the Irminger Gyre determines the transformation of the densest waters east of Greenland. We present a 19-year (2002-2020) weekly time series of hydrography and convection in the central Irminger Sea based on (bi-)daily mooring profiles supplemented with Argo profiles. A 70-year annual time series of shipboard hydrography shows that this mooring period is representative of longer term variability. The depth of convection varies strongly from winter to winter (288-1500 dbar), with a mean March climatological mixed layer depth of 470 dbar and a mean maximum density reached of $27.70 \pm 0.05 \text{ kg m}^{-3}$. The densification of the water column by local convection directly impacts the sea surface height in the center of the Irminger Gyre and thus large-scale circulation patterns. Both the observations and a Price-Weller-Pinkel (PWP) mixed layer model analysis show that the main cause of interannual variability in mixed layer depth is the strength of the winter atmospheric surface forcing. Its role is three times as important as that of the strength of the maximum stratification in the preceeding summer. Strong stratification as a result of a fresh surface anomaly similar to the one observed in 2010 can weaken convection by approximately 170 m on average, but changes in surface forcing will need to be taken into account as well when considering the evolution of Irminger Sea convection under climate change.

Plain Language Summary

The Atlantic circulation brings warm, lighter waters northwards in the upper part of the ocean, and colder, denser waters southward in the lower part of the ocean, creating a stable, stratified water column. East of Greenland, in the Irminger Sea, cooling by the atmosphere can transform these warm, lighter waters into the denser, deeper waters, which will eventually mix with deeper waters and flow southwards. To better understand how this transformation works and varies from year to year, we study measurements from instruments moored throughout the water column in the Irminger Sea between 2002 and 2020. We describe the progression of the average winter transformation and examine why transformation is stronger in some winters than in others. Overall, we find that the strength of winter cooling is three times as important as the stability of water column, a measure of its resistance to transformation, in the summer before. This finding will be important to better predict how the Atlantic circulation will develop in the future as a result of climate change.

1 Introduction

Deep convection, the process by which buoyant surface waters are transformed into denser waters by surface cooling (Marshall & Schott, 1999), is important for the Atlantic Meridional Overturning Circulation (AMOC). Eventually, through sinking along the boundaries (Katsman et al., 2018), these dense waters contribute to the Deep Western Boundary Current, which forms the deep southward branch of the AMOC. In model studies, the changes in strength of convection in the Subpolar Gyre are often linked to changes in AMOC strength, with many studies focused on deep convection in the Labrador Sea (Wood et al., 1999; Eden & Willebrand, 2001; Böning et al., 2006; Zhang et al., 2019).

Since 2014, the strength of the AMOC in the Subpolar Gyre has been measured by the Overturning in the Subpolar North Atlantic Program (OSNAP) array (Lozier et al., 2019; Li et al., 2021). The OSNAP array consists of two legs, OSNAP West crosses the Labrador Sea from Canada to Greenland and OSNAP East extends from Greenland eastward through the Irminger Sea, Iceland Basin and Rockall Trough to the European shelf. The results from OSNAP show that the eastern basins contribute most to both the total overturning strength as well as the variability of the overturning (Lozier et al., 2019; Li et al., 2021). Petit et al. (2020) showed that variability in subpolar overturning strength is linked to water-mass transformation by surface forcing over the Irminger and Iceland basins. Chafik et al. (2022) found that the link between Irminger Sea density and AMOC strength observed in the mooring data also existed in a longer (1993-2018) reanalysis time series and deemed the Irminger Sea to be the center of action for the subpolar AMOC. Furthermore, it is not the boundary currents that contribute most to the variability, but the eastern open-ocean basins (Li et al., 2021).

The density in the Irminger Sea is strongly affected by local convection. The occurrence of deep convection in the Irminger Sea was mentioned originally by Nansen (1912) and Sverdrup et al. (1942). After a long period of disinterest, the causes of which are detailed by Pickart et al. (2003), convection in the Irminger Sea received renewed attention with a series of studies on eventful convection years in the 2000s (de Jong et al., 2012; Piron et al., 2015; de Jong & de Steur, 2016; Piron et al., 2017; de Jong et al., 2018). These studies used data from moorings in the central Irminger Sea as well as Argo data to determine mixed layer depths. They showed that convection down to depths of 1600 m can occur and that convection is mainly driven by strong winter air-sea heat fluxes. Longer time series of near-annual hydrographic data (van Aken et al., 2011) paint a similar picture, with evidence of strong convection seen in oxygen concentrations and potential vorticity in the Irminger Sea during periods of strong positive North Atlantic Oscillation (NAO), similar to findings for deep convection in the Labrador Sea (van Aken et al., 2011; Yashayaev, 2007). Josey et al. (2019) proposed that a combination of a positive NAO and an East Atlantic Pattern (EAP) that is weaker than the NAO is linked to a higher occurrence of tip jets over the Irminger Sea (Moore, 2003; Moore & Renfrew, 2005) and therefore is linked strong local winter cooling.

However, strong surface forcing does not necessarily equate to strong convection. There have been periods in the observed record when convection was suppressed in the Labrador Sea by strong surface stratification during periods of strong surface forcing (Belkin et al., 1998; Gelderloos et al., 2012). Anomalously fresh near-surface layers, termed Great Salinity Anomalies, were suggested to suppress convection in the Labrador Sea from 1968 to 1972 and from 1981 to 1985 (Lazier, 1980; Dickson et al., 1988; Straneo, 2006; van Aken et al., 2011). However, this period was recently revisited by Kim et al. (2021), and their model simulations show that reduced surface fluxes may have had a larger role in the reduction of convection than the anomalously strong stratification. Less is known about the effect of the 1960s and 1980s Great Salinity anomalies in the Irminger Sea, although van Aken et al. (2011) suggest some moderate convection may have occurred in the early 1980s. The first analysis on the effect of a fresh anomaly on the stratification in the Irminger Sea by Bilo et al. (2022) found that the anomaly must have contributed partially to the weaker convection in the winter of 2019. Furthermore, the stratification in the region is projected to increase due to global warming and increased freshwater input from Greenland's Ice Sheet. Thus, Irminger Sea convection may be

inhibited by strong stratification more often or even permanently, potentially weakening the subpolar AMOC and have consequences for climate around the North Atlantic (Boning et al., 2016). It is therefore important to understand the variability of convection in this important region of the Subpolar Gyre and its dependence on surface forcing and stratification.

This paper aims to present a comprehensive description of convection in the central Irminger Sea and its variability based on a high temporal resolution multi-mooring time series supplemented with Argo records. The mooring time series covers the period from 2002 to 2020, which includes both periods of weak (< 500 m) and strong (> 1000 m) convection. We then place this 19-year record in the longer term context using a multi-decadal time series from near-annual hydrographic sections from 1950 to 2020. The relative importance of atmospheric forcing versus stratification as driving forces of Irminger Sea convection strength variability is investigated using the mooring data as well as results from the one dimensional Price, Weller, Pinkel (PWP, Price et al., 1986) mixed layer model.

Section 2 presents the data sets used in this study and details the processing methods. In Section 3.1 we provide a climatological description of convection in the Irminger Sea based on the 19-year time series. Section 3.2 discusses the interannual variability in the hydrography and convection observed in this record and takes a first look at the dependence of convection strength on ocean stratification versus atmospheric forcing. In Section 3.3 we investigate the role of stratification versus surface buoyancy forcing in more detail using the PWP model. Section 4 contains the discussion and conclusions.

2 Data and Methods

2.1 Hydrographic profile data from moorings and Argo floats

The record presented here is composed of data sets from three individual moorings in the central Irminger Sea that partially overlap in time: the Long-term Ocean Circulation Observations (LOCO) mooring, the Ocean Observatories Initiative (OOI) profiling HYPM mooring, and the Central Irminger Sea (CIS) mooring. Additionally, we include Argo profiles from a region around the moorings (Fig. 1).

The LOCO mooring, maintained from summer 2003 through summer 2018 by the Royal Netherlands Institute for Sea Research, was located in the center of the cyclonic circulation of the Irminger Gyre at approximately 59.2°N and 39.5°W (Fig 1.; de Jong et al., 2012; de Jong & de Steur, 2016; de Jong et al., 2018). The OOI HYPM profiling mooring (de Jong et al., 2018) is located slightly to the north of the LOCO position at 60°N and 39.5°W . The OOI profiler record presented here covers the 2014 to 2020 period. Both the LOCO and OOI moorings were outfitted with a McLane moored profiler (MMP) that records CTD (conductivity, temperature, depth) profiles at high vertical resolution along the mooring cable in the 150-2400 m interval for LOCO and the 230-2500 m interval for OOI. The time resolution for the MMP profiles varies from several time per day (LOCO deployment in summer 2011) to daily (other LOCO deployments) to once every two days (for OOI). Detailed data processing and quality control of the MMP data is described in de Jong et al. (2012). Special care is taken to correct for sensor drift of the conductivity sensor over the deployment using shipboard CTD data in order to obtain a

consistent salinity record over the whole period. Absolute salinity (SA), conservative temperature (CT) and potential density with respect to the surface (σ_0) were derived from the profiles using the TEOS-10 toolbox (www.teos-10.org).

The CIS mooring, located between the LOCO and OOI moorings at 59.5°N and 39.8°W, was maintained by GEOMAR from 2002 to 2016. It was outfitted with instruments at fixed depths (de Jong et al., 2018) rather than a moving platform like the MMP. As a result, the CIS profiles have a lower vertical resolution than the LOCO and OOI moorings, allowing for less accuracy in determining stratification and especially in locating the bottom of the mixed layers in winter. Therefore, we mainly use the CIS mooring data when no higher-resolution profiles are available. This is primarily in 2002–2003 before the start of the LOCO deployment and at times when there are gaps in the records of the higher-resolution LOCO and OOI moorings.

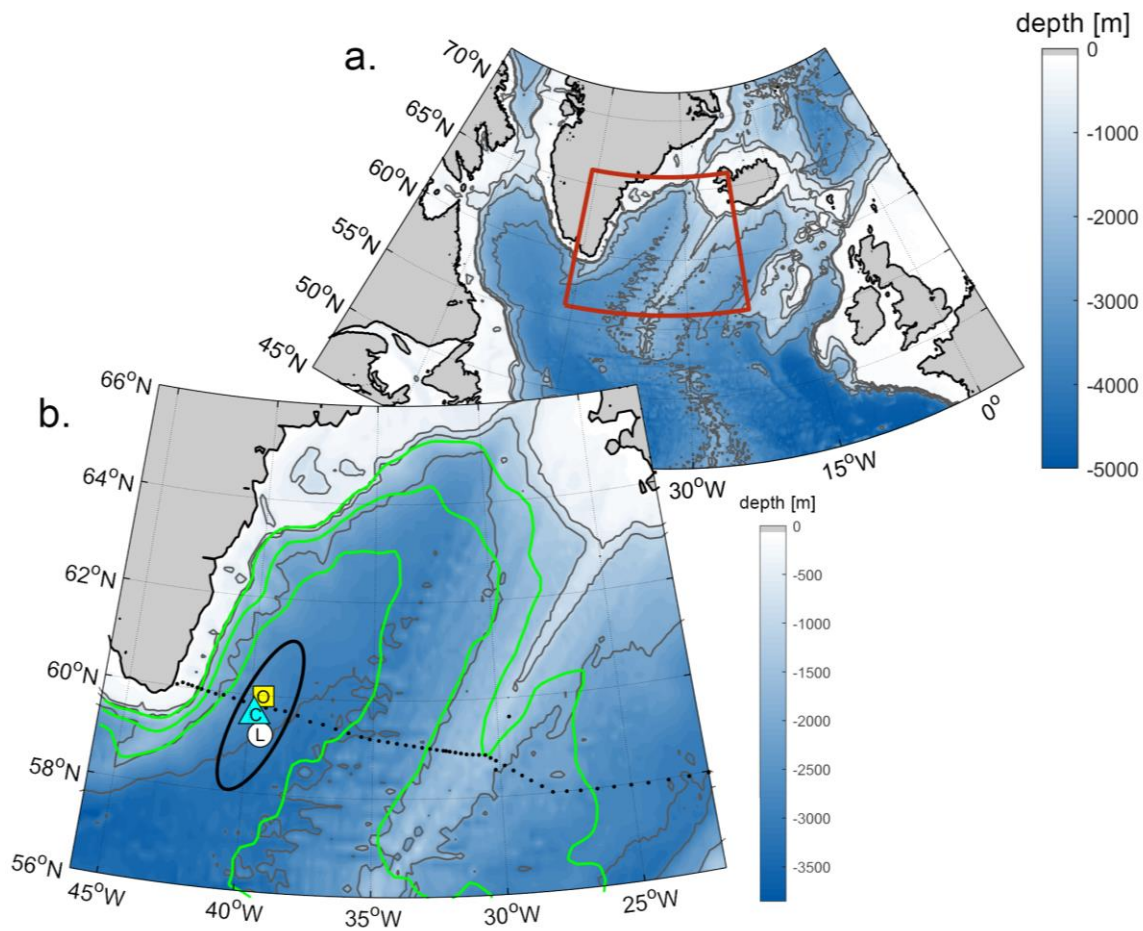


Figure 1. Maps of the study area and mooring locations. **a)** Overview map of the bathymetry of the northern North Atlantic. The Irminger Sea is enclosed by the red box. **b)** Zoom in of the red box with mooring locations in the central Irminger Sea indicated; white circle for LOCO, yellow square for OOI, cyan triangle for CIS and black dots indicate the OSNAP array. Argo profiles were collected within the area enclosed by the black ellipse. Sea surface height contours are plotted in green at 5 cm intervals.

Argo float profiles, with similar vertical resolution of the MMP profilers, were used to provide data in the near surface layer of the water column not covered by the MMPs. Argo profiles were selected in an ellipse around the center of the mooring positions, with a long axis distance of twice the north-south distance between the OOI and LOCO moorings, and a short axis of twice the east-west distance between these two moorings (Figure 1). The ellipse is aligned with the continental shelf of Greenland and the sea surface height contours, which ensures that the data represents changes over time in the weakly stratified central Irminger Gyre and excludes spatial differences arising from the more buoyant boundary currents. Argo floats typically record a profile every 10 days, but the amount of profiles in the study area depends on the number of floats present in the Irminger Sea each year. Over the years 2003 to 2020 there were on average 34 ± 21 (standard deviation) profiles per year recorded in the area enclosed by the ellipse. More details on number of available mooring and Argo profiles is presented in supporting information S1.

We composed a merged multi-mooring/Argo record to investigate hydrographic changes in the central Irminger Sea over the 2002-2020 period. This record was constructed as follows. Individual SA and CT profiles were subsampled vertically by averaging within 25dbar intervals. Next, profiles were averaged in time by applying a 1-week moving window. If LOCO, OOI or Argo profiles were available only these were used, otherwise the lower vertical resolution CIS data (when available) was used. This vertical and temporal smoothing removed small differences between the profiles that originate from their offset locations, while maintaining the seasonal and interannual variability that we are interested in here. The resulting weekly profiles in this merged record were extended to the surface using 1) sea surface temperature (SST) data from the fifth generation European Centre for Medium-Range Weather Forecasts atmospheric reanalysis product (ERA5), 2) a salinity time series based on the upper 50 m of Argo profiles, and 3) salinity and temperature records starting in 2014 from the near-surface instruments (12 m) at the OOI SUMO mooring, located right beside the OOI HYPM mooring (de Jong et al., 2018). The resulting time series of CT, SA and σ_0 covers the period from January 1st 2002 to December 31st 2020. The Brunt-Väisälä frequency (N^2) was derived from the weekly SA and CT profiles using the TEOS-10 toolbox in order to determine the Potential Vorticity (PV) as $PV = \frac{f}{g} N^2$.

We use mixed layer depth (MLD) as an indicator of local convection strength. MLDs were determined separately for each individual profile of the LOCO, OOI, CIS moorings and for each Argo profile. The turbulent mixing during convection homogenizes the water column properties, thereby characterizing a profile of a mixed layer by a nearly vertical profile of the hydrographic properties (CT, SA and σ_0). At the bottom of the mixed layer, the profile transitions to the stratified profile of the deeper water column not affected by mixing. Because of the weak stratification at mid-depth (500 to 1500 dbar) throughout the year, it is difficult to determine the bottom of the mixed layer from density alone in the Irminger Sea—there is nearly no density transition as the current year's mixed layer reaches into the previously convected water masses at mid depth. Therefore, the additional information provided by temperature and salinity is needed to determine MLDs, as these variables often do show transitions between water masses while density does not.

An initial pass of the algorithm of Holte et al. (2017), which determines the MLD based on a straight line least-squares fit to temperature, salinity and density, provided a first separation into

profiles with and without mixed layers. Profiles were selected for which the determined MLDs of temperature and salinity were within 50 dbar of each other and the MLD for density was similarly within 50 dbar or deeper. For profiles that did not extend to the surface, as is the case for most of the mooring data, MLDs could only be determined from MLDs extending deeper than 75 dbar. Even with these requirements, the algorithm still selected MLDs that did not pass manual inspection; particularly for profiles that showed a transition that appeared like the bottom of a mixed layer but showed too much variability within the water column above the algorithm-determined MLD. These are likely remnants of mixed layers that were formed recently and horizontally advected to the moorings. However, since our interest here is in active mixing at the moorings, these profiles were removed. Out of a total of 4683 profiles from the months in which mixed layers typically can occur (December through April), 688 profiles (15%) showed a MLD deeper than 200 dbar that passed inspection (Table 1). Lastly, time series of MLDs at each platform were merged into one three-day average MLD time series for the central Irminger Sea.

Table 1. Overview of number of winter profiles and profiles with mixed layers.

	Years covered	All profiles	Winter profiles	MLD > 200 dbar (after inspection)
LOCO mooring	2003-2018	4969	1918	283
OOI mooring	2014-2020	1168	535	75
CIS mooring	2002-2016	4769	1966	273
Argo	2003-2020	969	264	57
Total		11875	4683	688

2.2 Ocean and atmospheric buoyancy time series

We are interested in the role of stratification versus the role of surface forcing in the interannual variability of Irminger Sea convection. To quantify the stratification, we calculated the buoyancy of the water column between different depths from the mooring/Argo record as well as from the decadal hydrographic record. The water column buoyancy (B_{ocean}) in J kg^{-1} between depth z_1 and z_2 is defined as:

$$B_{ocean} = \frac{g}{\rho_0} \int_{z_1}^{z_2} \sigma_0(z_2) - \sigma_0(z_1) dz,$$

where g is the gravitational acceleration, $\sigma_0(z)$ is the potential density profile and ρ_0 is a fixed reference density (Schmidt and Send, 2007; Bilo et al., 2022).

The surface buoyancy forcing ($B_{forcing}$) in J kg^{-1} resulting from atmospheric fluxes is defined as:

$$B_{forcing} = \frac{g\alpha}{\rho_0 C_p} Q - \beta g S_0 (E - P),$$

where α is the thermal expansion, C_p is the heat capacity, Q is the net atmospheric heat flux, β is the haline contraction of seawater, S_0 is the surface salinity, E is evaporation and P is precipitation. With the first term on the right representing the atmospheric thermal forcing role and the second term representing atmospheric freshwater forcing, the role of heat versus

freshwater forcing will be investigated by evaluating the two right hand terms separately. To calculate $B_{forcings}$, net shortwave and net longwave radiation, sensible and latent heat fluxes (for Q), and total precipitation and evaporation (for $E-P$) fields from the ERA5 atmospheric reanalysis were downloaded from the Copernicus Climate Data Store (<https://cds.climate.copernicus.eu/cdsapp#!/dataset/reanalysis-era5-single-levels?tab=overview>). Daily fields were used for the 2002-2020 period and monthly fields were used for 1950-2020. At each time step, Q and $E-P$ were averaged over our study region (the ellipse in Figure 1) as well as obtained directly from the grid point closest to the LOCO mooring location. Two time series are nearly identical, with correlations of 0.996 (for Q) and 0.97 (for $E-P$) and differences in the mean of 2% (for Q) and 5% (for $E-P$) with the point values being higher than the area average. In the remainder of this manuscript we will use the fluxes averaged over the ellipse in Fig.1.

2.3 Decadal time series from shipboard hydrography

To put the variability over the 19 years of the mooring record into longer term context, we extended the 1950-2009 multi-decadal time series of (near-)annual hydrography for temperature, salinity, and density in the central Irminger Sea described by van Aken et al. (2011) to 2020. This time series includes historical data (from sample bottles) for the pre-World Ocean Circulation Experiment (WOCE) period from 1950 until 1989, and high-quality hydrographic data collected during near-annual repeat CTD surveys of the AR7 hydrographic section, the original survey line on which the location of the OSNAP array was based, from 1990 onwards (<http://cchdo.ucsd.edu/>). CTD data from 2014 onwards was mainly collected during the cruises that serviced the OOI and OSNAP moorings. The AR7 East (AR7E) hydrographic sections were surveyed predominantly in summer (April to October) to avoid ice conditions and the storm season. The time series therefore represents stratified summer conditions and does not capture seasonal changes or winter MLDs. However, it does capture the inter-annual through decadal changes in upper ocean stratification as well as changes in the low PV conditions at mid-depths resulting from strong winter convection (described in more detail in van Aken et al., 2011).

Figure 2 shows the 70-year record with the mooring period indicated at the end. At first glance, the hydrography of the mooring period (panels 2b through 2e) does not stand out as exceptional compared to the longer record; however, this period included both exceptionally strong stratification around 2005 and exceptionally low stratification towards the end (panel 2a). This change in stratification was mainly temperature driven, with the early 2000s being warm and the late 2010s being colder. The atmospheric forcing exhibits high interannual variability (panel 2a), but the 5-year running mean of the forcing shows that overall the mooring period was comparable to the overall mean. Since the variability in the hydrography and atmospheric forcing during the mooring period is comparable to the longer term variability, the climatology allowed by the higher temporal resolution data will also be representative of conditions in the Irminger Sea over the last 70 years. Because the last 19 years cover nearly the full range of stratification observed over the last 70 years, our investigation of the respective influence of stratification versus forcing on convection strength is likely generalizable to the full 70 year record.

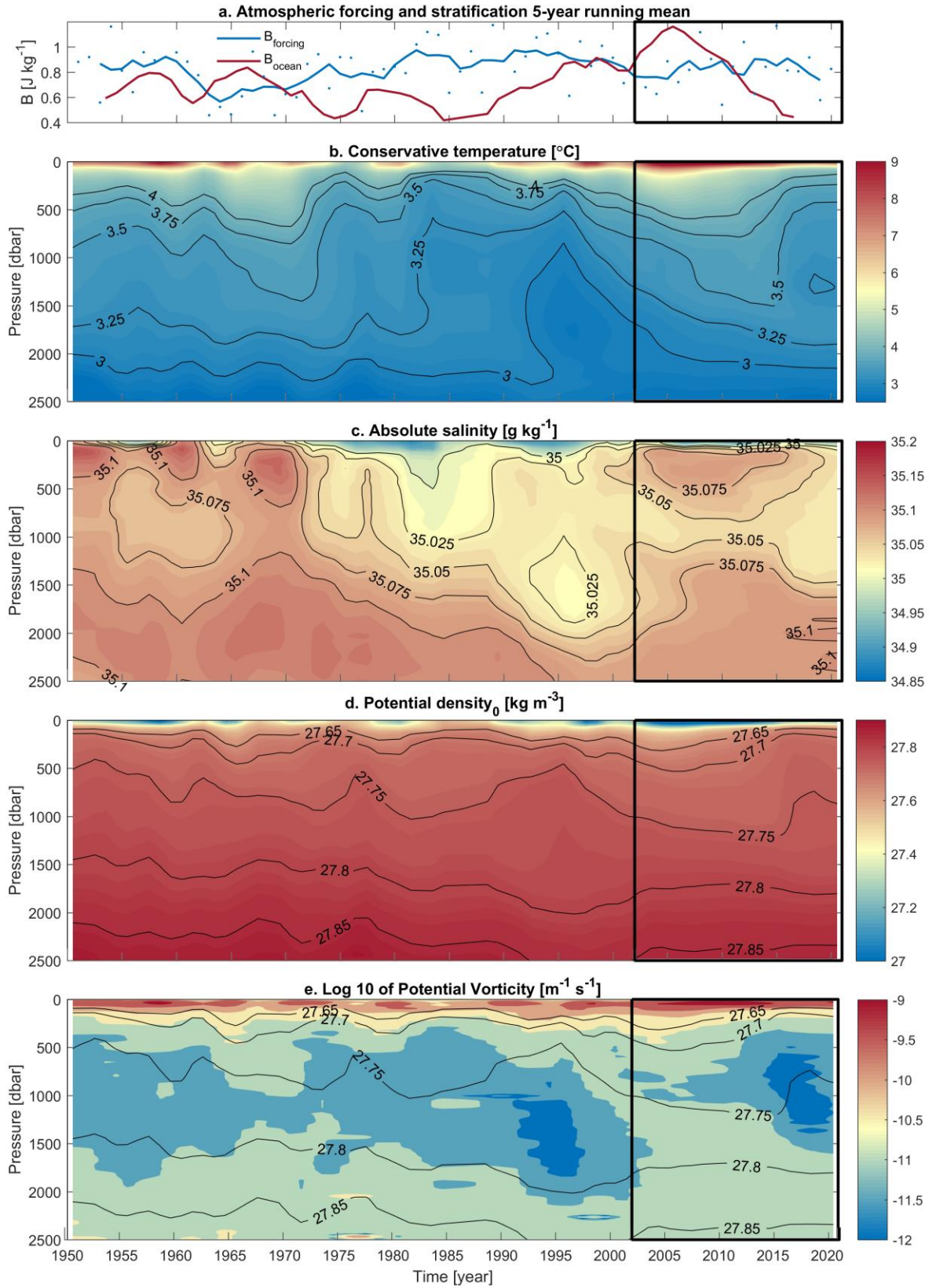


Figure 2. Central Irminger Sea multi-decadal hydrographic time series of **a.)** 5-year running mean values of the stratification over the upper 1000 m (red) and the cumulative atmospheric forcing (blue). Annual forcing values shown as blue dots. **b.)** conservative temperature, **c.)** absolute salinity, **d.)** potential density and **e.)** potential vorticity. The mooring period is indicated with the black box.

2.4 The PWP mixed-layer model

We use a one-dimensional mixed-layer model to distinguish between the roles of atmospheric forcing and stratification on the variability of winter convection in the Irminger Sea. The Price, Weller and Pinkel or PWP model (Price et al., 1986) has previously been used in the North Atlantic by Lazarevich et al. (2004). In that study, the authors demonstrated that the PWP model was capable of reproducing year-long float-observed sea surface temperatures to within 1°C, as well as the timing of the ventilation and stratification of the mixed layer.

Briefly, the PWP model is a vertical, bulk mixed-layer model that simulates the evolution of water-column temperature and salinity as a result of atmospheric forcing. The model requires an initial temperature and salinity profile and inputs of surface heat, freshwater and momentum fluxes. Precipitation, long-wave radiation, sensible heat, and latent heat are input at the ocean surface. Incoming shortwave radiation was modeled as a function of depth according to Paulson and Simpson (1977) using the optical properties of a 1b water type (Jerlov, 1968). Static instability in the mixed layer is adjusted by entraining water from below until stability ($dp/dz \geq 0$) is achieved. Bulk and gradient Richardson numbers are determined, and if found below critical thresholds (bulk < 0.65 and gradient < 0.25), deeper water is entrained and the process is repeated until vertical stability is achieved (Price et al., 1986). The result is a bulk mixed layer in which all properties (e.g., temperature, salinity, chemical species) are uniformly distributed. See Price et al., (1986) for more details.

In this study, PWP model experiments were performed for the Irminger Sea, each with different initializing water-column conditions and surface forcing records. On September 1 of each year, model runs were initialized using the mean SA and CT profiles collected during the period of maximum water-column stratification, occurring in the Irminger Sea from mid-August to mid-September. PWP experiments were forced with inputs of surface heat, freshwater and momentum fluxes from ERA5 Reanalysis products for the Irminger Sea (60°N, 39.5°W; Hersbach, H. et al., 2018). ERA5 Reanalysis products for 6-hour intervals were interpolated to 1-hour intervals and used to force the model for a year. At each time step, profiles of temperature, salinity, and momentum were determined, with model outputs of MLD and water-column temperature, salinity and density being saved every 3.5 days. Density was calculated using the full equation of state. Three types of PWP experiments were performed:

Experiment type 1: Yearly reconstruction of the observed MLD variability from 2003-2020. Each year, the PWP model is initialized with the observed maximum-stratification water-column profiles of that particular year and forced with the corresponding year-long surface fluxes.

Experiment type 2: Role of varying water-column stratification in interannual MLD variability. PWP model runs are initialized each year with the observed maximum-stratification water-

column profiles from that year. Surface forcing is not varied, rather the surface fluxes of one winter are used to force all winters.

Experiment type 3: Role of varying surface forcing in interannual MLD variability. The stratification is not varied, the PWP model runs are initialized with the same water-column profiles each year, but forced with the unique surface fluxes of the particular year.

Multiple version of experiment type 2 (using various example winters) and type 3 (using various example stratifications) have been done. In total, 137 year-long PWP runs spanning the full range of stratification and forcing conditions were done.

3 Results

The data sets presented above provide an unique opportunity to describe convection in the central Irminger Sea, to study its variability over interannual and decadal time scales, and to investigate the respective driving forces of variability. The mooring record documents several periods of weak convection ($MLD < 500$ m) as well as several periods of strong ($MLD > 1000$ m) convection (described in more detail in Section 3.2).

3.1 Climatology of 2002-2020 Irminger Sea convection

In Figure 3, we present seasonal climatologies for the surface buoyancy forcing, MLD, Absolute Dynamic Topography (ADT) and the mixed-layer temperature, salinity and density. ADT was retrieved from the ARMOR 3D 0.25° data set at Copernicus (Mulet et al., 2012). Both the monthly mean climatological values with standard deviations, as well as the daily means for each day of the year are shown. Additionally, we show the daily climatology of the SST, salinity in the upper 50 m (Argo, OOI surface mooring), and derived density over the same time period. Note that all the shallow (< 100 m) MLDs in summer are from Argo profiles as these cannot be determined from the subsurface mooring profilers.

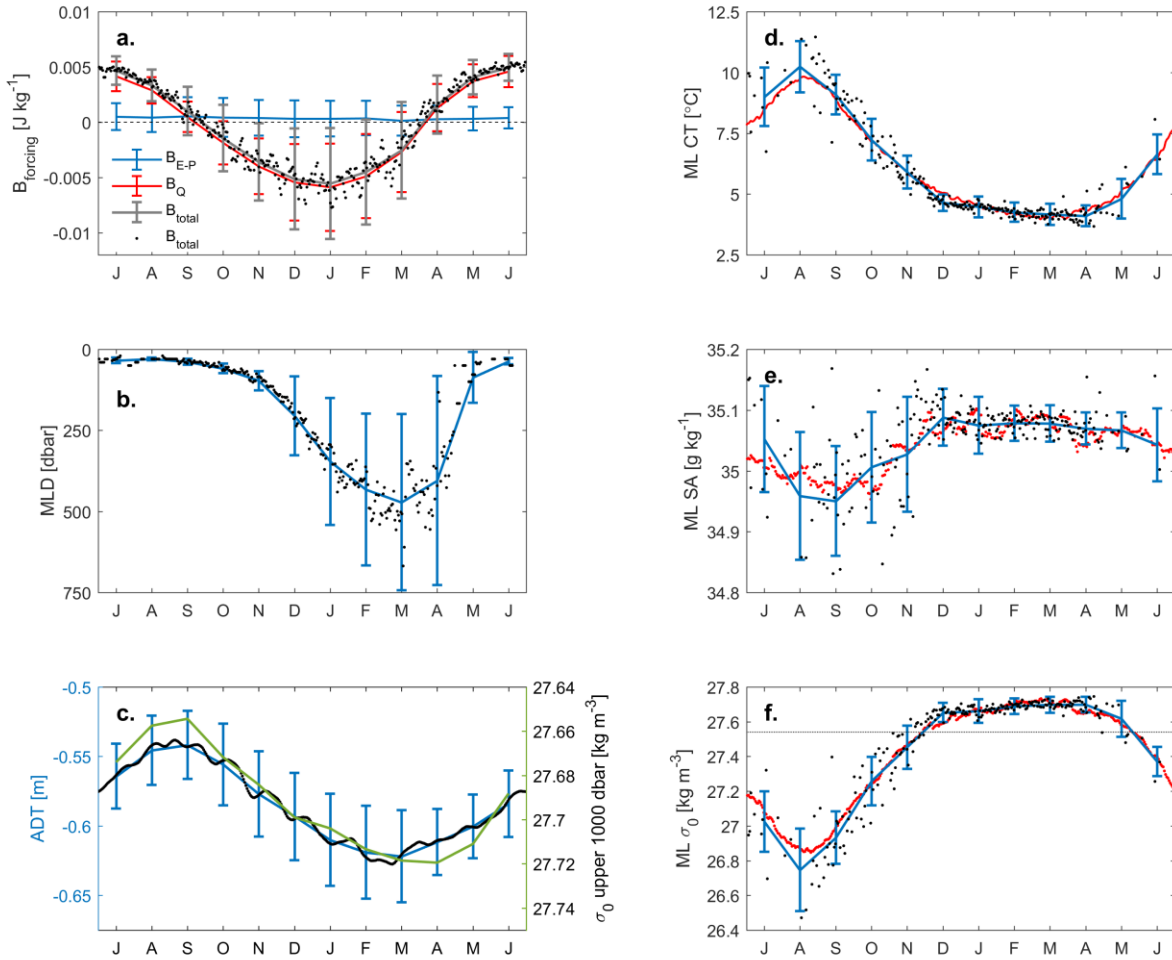


Figure 3. Seasonal climatologies of properties associated with convection in the central Irminger Sea. A start date of 1 July was chosen to show evolution of MLDs through a complete winter. Black points in each of the panels indicate daily means with the lines and error bars representing the monthly mean and standard deviation. **a.** Seasonal climatology of surface buoyancy forcing (J/kg). Plotted are the component derived from heat fluxes (B_Q in red), freshwater fluxes (B_{E-P} in blue) and the total atmospheric buoyancy flux (B_{total} in grey and black). Zero line is dashed. **b.** Mixed layer depth (MLD, dbar). **c.** Absolute dynamic topography (ADT, m in blue and black) and mean potential density over the upper 1000 dbar of the water column (σ_0 , kg m^{-3} in green). **d.** Mixed layer conservative temperature (ML CT $^{\circ}\text{C}$ in blue and black) and SST (in red). **e.** Mixed layer absolute salinity (ML SA, g kg^{-1} in blue and black) and daily upper 50 m absolute salinity (in red). **f.** Mixed layer potential density (ML σ_0 , kg m^{-3} in blue and black) and potential density calculated from SST and 50 m salinity (in red). The grey line is the potential density of the maximum overturning for OSNAP East (27.54 kg m^{-3}).

The seasonal climatology (Fig. 3) shows that heat fluxes largely determine the total buoyancy lost to the atmosphere in winter. The Irminger Sea gains buoyancy through freshwater year round, but the atmospheric freshwater fluxes are an order of magnitude smaller and fairly constant throughout the year. The large standard deviations in winter, mainly seen in the heat and total fluxes, indicate both intermittency in heat fluxes (short lasting high flux events alternating with calm days) and interannual variability (discussed in more detail in section 3.2). Heat fluxes add buoyancy from April through September, but remove more buoyancy from October to

March through stronger heat fluxes, thus leading to a net loss of heat and buoyancy over the year.

Even though the Irminger Sea gains buoyancy over summers, it is a relatively windy region- year round (Duyck & de Jong, 2022), and shallow mixed layers are common throughout the year (Fig. 3b). The atmospheric freshwater forcing (net gain) is collected in this upper layer (Sterl & de Jong, 2022) creating a minimum salinity around September. This thin fresh layer warms through spring and summer, reaching its highest temperature and lowest density in August (panels 3d., 2e. and 2f.). In September, the ocean starts to lose heat to the atmosphere and the surface and ML temperature decrease quickly. Through October and November, the surface heat fluxes increase further, but are mainly still removing heat from the upper 100 dbar. With most of the heat removed from this upper layer, and strong heat loss occurring from December to March, the climatological MLD gradually increases from 205 ± 122 dbar in December to 471 ± 271 dbar in March. Generally, heat loss weakens in April, leading to a sudden shallowing of the MLD. However, in strong winters that occasionally last through April, the MLD increases further leading to a bigger standard deviation for April (405 ± 322 dbar) compared to March. In May, the heat fluxes change sign and the ocean gains heat causing a sudden halt to convection. SST starts to increase and MLD decrease to (87 ± 79 dbar).

The hydrographic climatologies show that the density follows the changes in temperature. Temperature decreases steeply from a climatological maximum of 10.2 ± 1.0 °C in August to 4.6 ± 0.3 °C in December and then gradually decreasing further to a minimum of 4.1 ± 0.4 °C in April. The gradual decline during strong surface fluxes is due to the heat loss being spread over a thicker mixed layer. Sea surface temperature from satellite data follows the mixed layer temperature closely. The potential density changes from an August minimum density of 26.75 ± 0.24 kg m⁻³ to 27.65 ± 0.06 kg m⁻³ in December and then increasing gradually to a maximum in March and April of 27.70 ± 0.05 kg m⁻³. Salinity decreases through summer, due to accumulating freshwater from precipitation and possibly a freshwater export from Greenland. In September the climatological salinity is 34.95 ± 0.09 g kg⁻¹. The large standard deviation reflects large differences between different summers, as some were characterized by significantly fresher anomalies (Oltmanns et al., 2018; Bilo et al., 2021; Sterl & de Jong, 2022). Salinity increases as the mixed layer deepens below this fresh summer layer and reaches into the more saline Subpolar Mode Water (SPMW) underneath. However, there is a second inversion in the vertical salinity profile, with fresher waters at mid-depths (locally convective water from previous winters and Labrador Sea Water (LSW)). Thus, as mixed layers deepen beneath the SPMW into this fresher layer from December onwards the salinity gradually decreases.

Overall, the standard deviations of the hydrographic properties decrease as the MLD increases. This is also seen in records of instruments at fixed depths with higher temporal resolution (de Jong et al., 2018). It reflects the (nearly) absent gradients within the mixed layer, the changes in heat and freshwater applied at the surface being spread over a thicker layer, as well as the fact that this takes place over a substantial area, thus reducing lateral gradients. This vertical and lateral homogenization ceases as winter cooling ends and restratification sets in, leaving behind the characteristic homogeneous convective water mass at mid-depths with a typical low PV signature.

Sea surface height, or ADT, is largely a function of steric height and will be affected by changes over a large part of the water column. This is confirmed by the seasonal cycle of ADT that follows that of the density of the upper 1000 dbar of the water column. However, the timing of the minima are offset one month, with ADT increasing slightly before density does. This offset disappears if a layer of 250 dbar or shallower is used for the mean density (not shown), indicating that the onset of restratification of this upper layer causes the increase of ADT.

3.2 Interannual variability during 2002-2020 period

There is large interannual variability in MLD in the central Irminger Sea (de Jong et al. 2012), resulting in large standard deviations in the monthly climatology (Fig. 3). Here we investigate the interannual variability further using the 19-year mooring/Argo record. Figure 4 shows the merged mooring/Argo records of temperature, salinity, density, and potential vorticity with MLD, with the latter two giving the most insight into the strength of convection in each winter. We will denote winters by the last digits of the years in which they occur, for example the winter of 2002-2003 as 02-03.

At the start of the record in 2002, the water column was relatively fresh and a weak PV minimum can be seen around 700 to 1000 dbar. The first five winters (the winters of 02-03 to 06-07) did not see intense convection, with MLDs between 395 and 620 dbar. This layer restratifies fully in summer (Sterl & de Jong, 2022), and therefore these MLD did not make an imprint of low PV on the water column that remained after winter. During this period, the water column warmed and became more saline, continuing the ongoing restratification of the Irminger Basin after the intense convection in the 1990s (van Aken et al., 2011). The winters of 07-08 and 08-09 were the first winters in the mooring record where mixing reached just below 800 dbar and a low PV signature remained visible at these mid-depths. The next winter (09-10) had the shallowest mixing observed in the record, a mere 288 dbar, and was followed by another winter with fairly weak convection (500 dbar in 10-11). A winter with intense convection (998 dbar) followed in 2011-2012. Interestingly, during the next two winters (12-13 and 13-14) convection was weak (MLD of 572 and 650 dbar respectively), but an imprint can be seen in PV. This suggests that deeper mixing may have occurred nearby, after which low PV water were advected to the mooring location. Both the winters of 14-15 and 15-16 showed the strongest convection of the record, with MLD of 1500 and 1250 dbar, respectively. Convection remained strong through 16-17 and 17-18, with MLD of 880 and 1020 dbar. In the last two winters of this record, 18-19 and 19-20, convection was weak (408 and 650 dbar). The occurrence of intense convection during four consecutive winters (14-15 through 17-18), aided by the arrival of a fresh anomaly in the near surface layers (de Jong et al., 2020; Holliday et al., 2020; Bilo et al., 2021) reversed the trend of warming and salinification in the central Irminger Sea, with intermediate waters becoming colder and fresher. Despite the lower salinities, the cold character of the strong convection from 2014 to 2018 created a denser class of mid-depths waters in the Irminger Sea. A low PV signature of convection remains to be seen in the intermediate water even after the weaker convection of the last two winters.

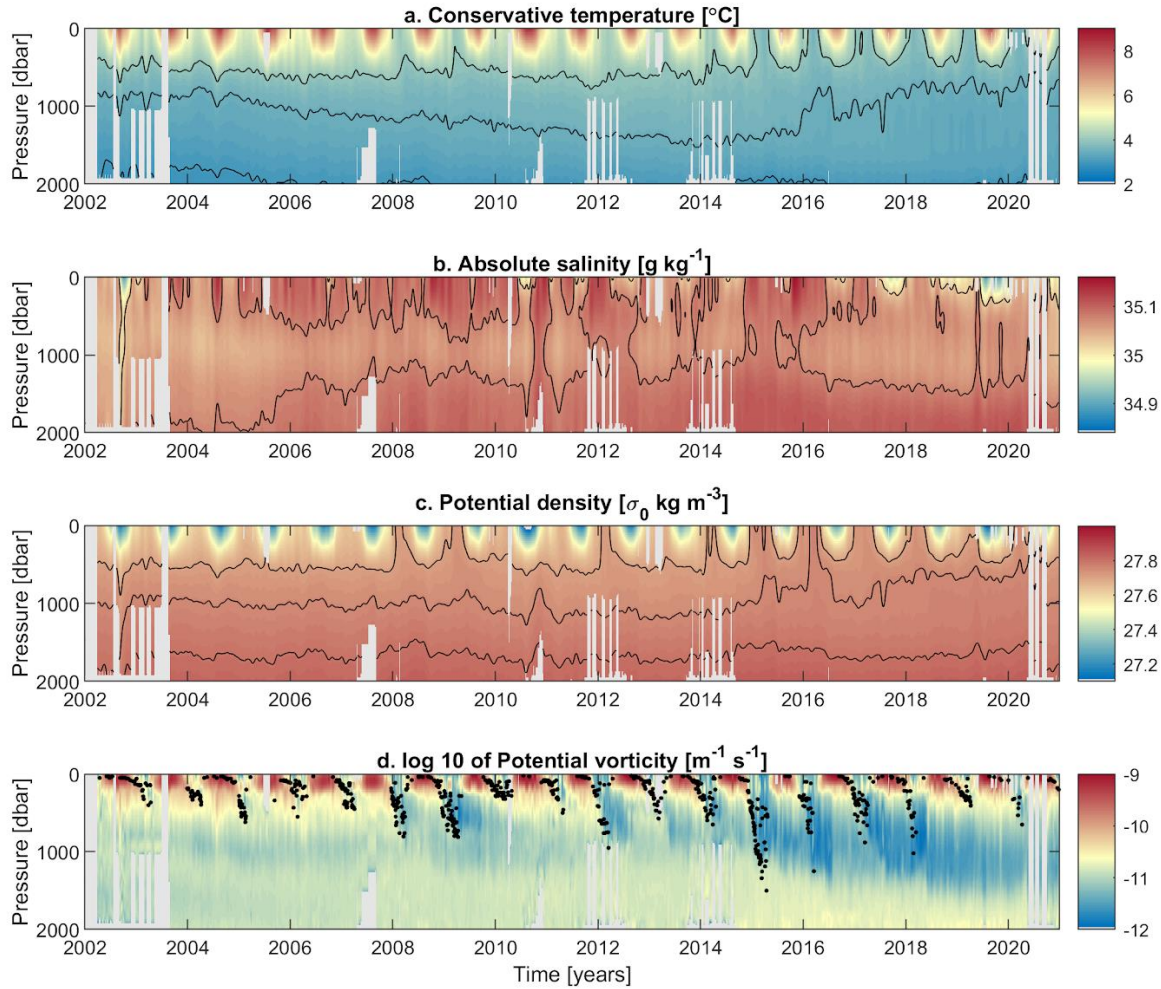


Figure 4. Merged mooring and Argo time series from 2002 to 2020. **a.)** Conservative temperature with black contours at 3, 3.5 and 4°C, **b.)** Absolute salinity with black contours at 35.025 and 35.075 g kg⁻¹, **c.)** Potential density (color), with black contours at 27.7, 27.75 and 27.8 kg m⁻³ and **d.)** Potential vorticity (in color) and mixed layer depth (black dots).

The impact of the interannual variability in convection on the density in the upper 1000 dbar of the water column, and thereby on ADT is clear from Figure 5. The density averaged over the upper 1000 dbar exhibits a strong seasonal cycle, with density in winter mixed layers setting the maximum density each year. The ADT time series follows that of upper 1000 dbar density. Winters with deeper MLD create denser convective waters, which depress the height of the sea surface further. The winters of 07-08 and 11-12 particularly showed steeper drops in ADT compared to the previous winter. Both the seasonal cycle and the interannual variability cause a strong correlation between ADT and density. The maximum correlations are found at the surface, with a correlations of -0.83 between 30-day low-passed σ_0 and ADT. After deseasoning these timeseries, by removing daily climatology, the correlation is -0.68. These correlations decrease approximately linearly with depth until they are about zero at 1200 dbar depth. This indicates that density of waters advected from the Labrador Sea, around 1000 dbar, does not contribute significantly in the local variability of σ_0 and ADT. Local processes in the upper part of the water column in the Irminger Sea, e.g. convection and restratification, set the ADT.

There is ongoing discussion concerning the relative roles of the surface buoyancy forcing versus the water column stratification in determining the mixed layer depth in the Irminger Sea (Bilo et al. 2022). Figure 5 shows the interannual variability of the cumulative heat, freshwater and total buoyancy forcing over each winter, as well as the time series of water-column stratification of the upper 1000 dbar. Even though there is considerable variability in freshwater fluxes (Fig. 5b.), the variability in heat fluxes dominate the interannual variability of the total buoyancy loss in winter. The strongest winters in this 2002-2020 record are the winters of 07-08, 11-12 and 14-15. All these winters showed a deepening of the MLD with respect to previous years. There are a number of years with weak surface buoyancy forcing, particularly 03-04, 09-10, 12-13 and 18-19. These are also the years with shallowest MLD (Fig. 5c.) and relatively small winter drops in ADT (Fig. 5d.).

Not surprisingly, the water-column buoyancy also shows a clear seasonal cycle (Fig. 5b). We integrate B_{ocean} over the upper 1000 dbar of the water as this contains both the contribution to this seasonal cycle comes from the upper 500 dbar of the water column and the interannual signal in the layer between 500 and 1000 dbar. During periods of strong convection ($MLD \geq 800$ dbar) the buoyancy of the layer between 500 and 1000 dbar is reduced and minima are lower. The interannual variability in the restratification of the water-column buoyancy is small, with only a few years standing out as having a stronger stratification built up through summer. These are the summers of 2007, 2010 and 2019. The strengthening of stratification in these years is (at least partly) the result of larger than average atmospheric freshwater fluxes (Fig 5a) leading to an anomalously fresh and warm near surface layer. However, over most of the profile above 1200 m, temperature is the dominant driver of density changes (further explained in supporting information S2). A more thorough description of restratification in the Irminger Sea can be found in Sterl and de Jong (2022).

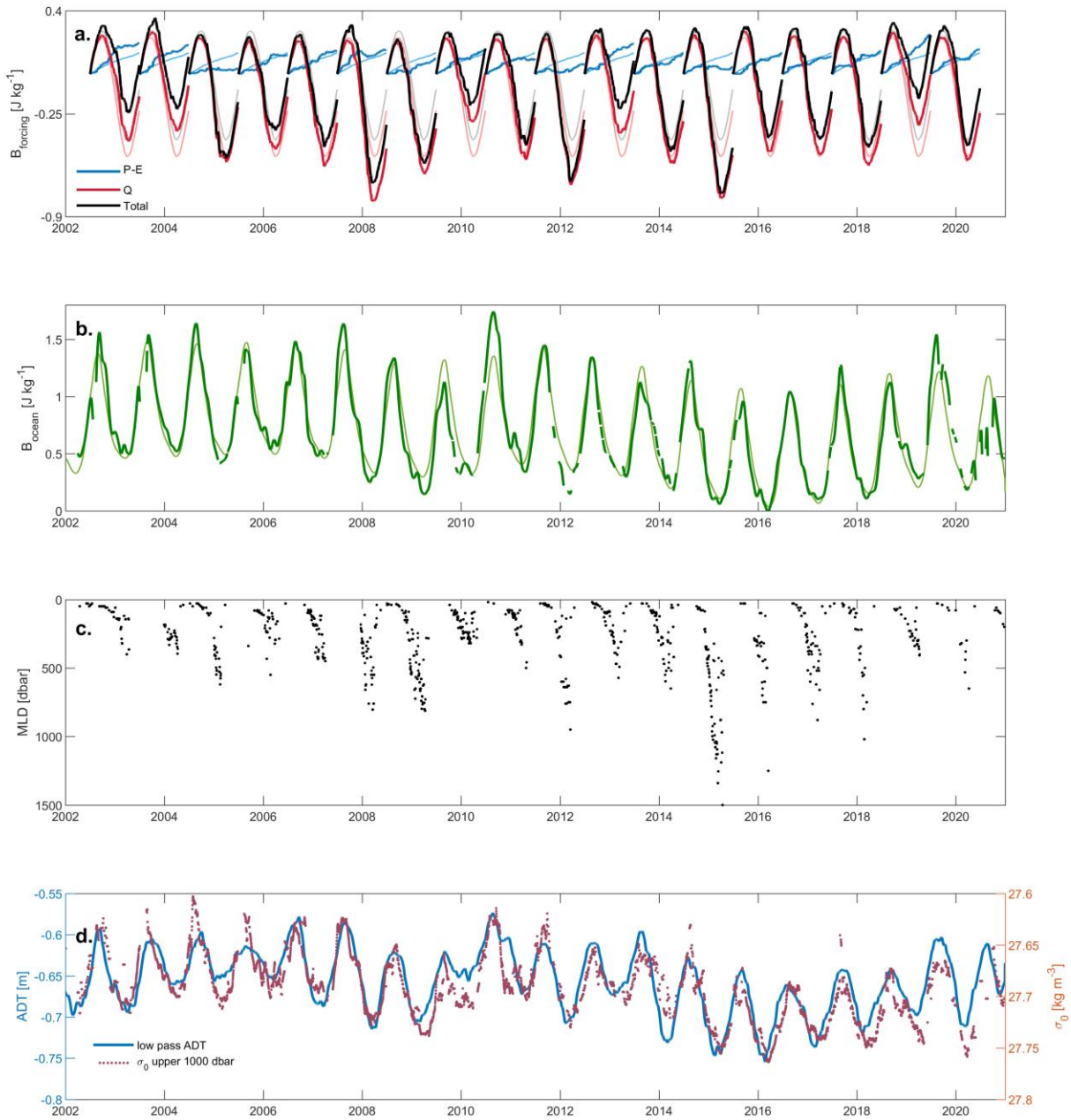


Figure 5. Cumulative surface buoyancy forcing starting at 1 July of each year, water column buoyancy, mixed layer depth, upper 1000 dbar density and ADT. **a.)** shows the total cumulative buoyancy forcing (thick black line) as well as the contribution of heat fluxes (Q , thick red line) and freshwater fluxes ($P-E$, thick blue line). Thinner lines of corresponding colors represent the seasonal climatology. **b.)** Water column buoyancy integrated between 1000 dbar and the surface (thick green line). Thin light green line is the seasonal climatology superpositioned on the low pass (3-year running mean) time series, highlighting years with stronger than average break down or build up of stratification. **c.)** Mixed layer depth. **d.)** Density averaged over the upper 1000 dbar of the water column (red dots), daily unfiltered ADT (m, light blue) and low-pass filtered (30-day running mean) ADT (m, thick blue line)

By distilling the data in Fig. 5 to annual extremes, we get a first insight into the relative importance of atmospheric forcing (B_{forcing}) versus stratification (B_{ocean}) to the MLD and the properties of the central Irminger Sea (Fig. 6). There is a strong correlation (Fig. 6a) between the total accumulated heat loss through winter and the annual maximum MLD in that winter but no significant correlation (Fig. 6b) between annual maximum summer stratification and the annual maximum MLD in the following winter. Deeper MLD result in a higher mixed layer density (Fig. 6c), with a progression from lighter and shallower mixed layers at the start of the record to deeper and denser mixed layers at the end. There is a very strong relation between the maximum MLD and the maximum stratification in the following summer (Fig. 6d). This means that the summer water column stratification is highly dependent on the amount of stratification removed in the previous winter, rather than that the MLD is dependant on the stratification. This finding is aligned with Sterl & de Jong (2022), who determined from reanalysis data that the restratification over the upper 600 m is fairly constant from year to year and mainly depends on the convection in the preceeding winter.

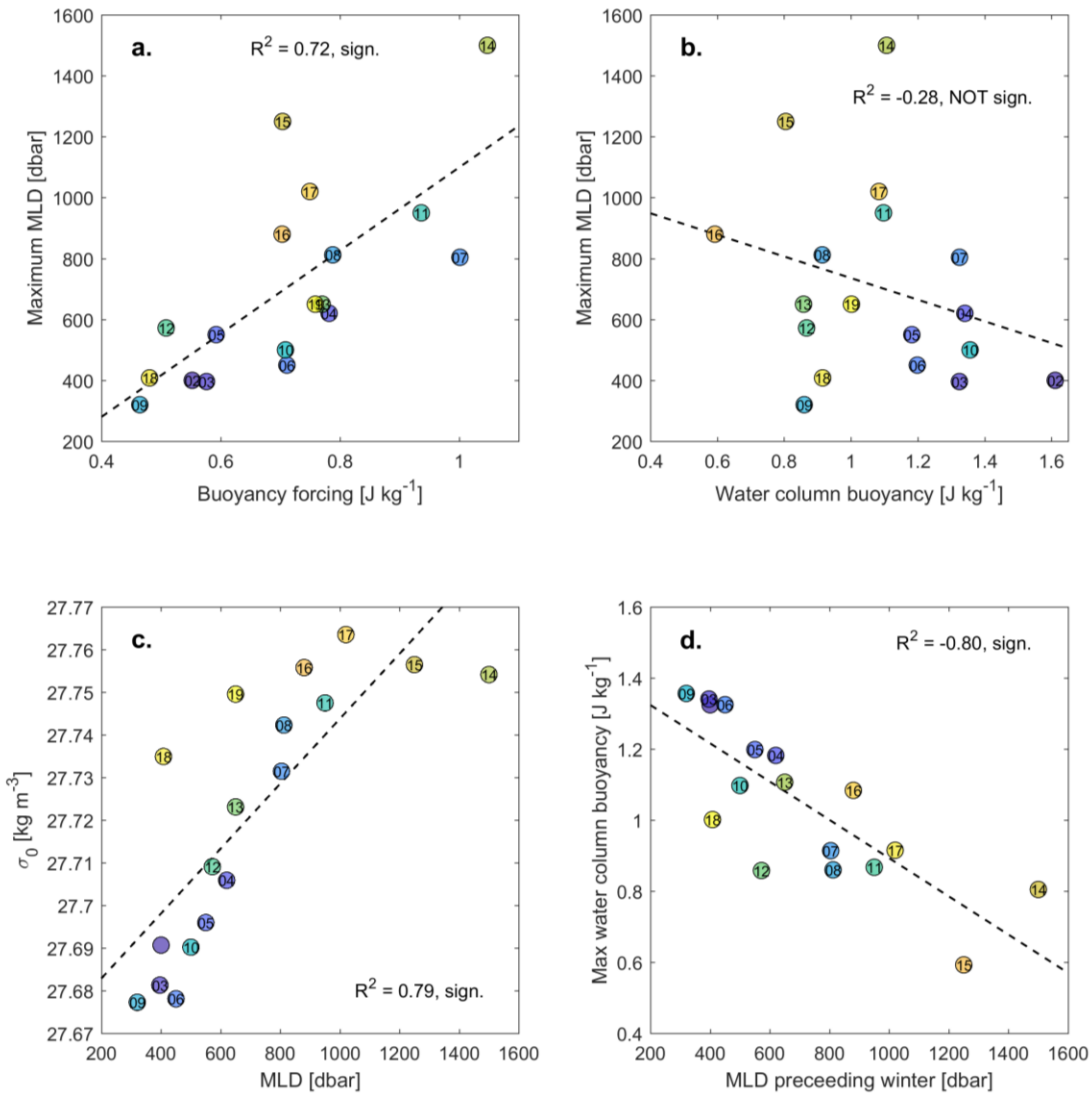


Figure 6. Scatter plots of interannual variability. **a.)** Annual maximum MLD against maximum cumulative surface buoyancy loss over winter (fall maximum – spring minimum in Fig. 5), **b.)** Annual maximum MLD against annual maximum water column buoyancy over upper 1000 dbar, **c.)** Annual maximum ML density against annual maximum MLD. **d.)** Annual maximum water column buoyancy over upper 1000 dbar against maximum MLD in the preceding winter. The color of the markers shows the progression through the record, but the digits of the year are also indicated. Correlations, and whether they pass a 95% significance test, are also indicated.

3.3 Role of forcing versus stratification in the PWP model

Three types of experiments were done with the PWP model to further test the sensitivity of the MLD to the atmospheric buoyancy forcing and the initial water column buoyancy. The first type of experiment (Fig. 7a) aimed to reproduce the observed variability in MLD was simulated by applying the unique surface forcing of each winter to a water column initialized with the observed maximum water column stratification of the preceding summer. The reproduced interannual variability in MLD matches the observed MLD quite well, although it tends to overestimate MLD in some years (especially 2010). The second type of PWP experiment aimed to show the role of variable surface forcing. In the example of Figure 7b, the unique surface forcing of each year was applied to the same stratification, namely the mean maximum water column stratifications over the record. By using identical initialization profiles for each year in these experiments, the interannual variability in the atmospheric forcing is maintained and the influence of varying stratification is removed. These runs match the observed MLD slightly better, with a slightly higher correlation and a lower root mean square error (RMSE) with the observed MLD record than the experiment using both the observed stratification and the observed forcing (Fig 7b, as compared to Fig. 7a). Somewhat surprisingly, this indicates minimal or no loss of model fidelity in reproducing the observed MLD record when the influence of interannually-varying stratification is removed. In particular, using the mean stratification reduced the MLD simulated for 09-10, and 15-16 through 17-18, which were over estimated in Fig 7a. The third type of experiment (Fig. 7c), aimed to show the role of varying stratification. The model was initialized in each year using the observed maximum stratification from that summer, but is forced with identical surface forcing in each year. In the example shown in Fig 7c, a normal year forcing is used. The year 2012-2013 was chosen as normal year as its cumulative surface forcing was close to the 2002-2020 mean cumulative surface forcing. We chose to use a representative individual winter's forcing for this experiment type rather than a climatological mean in order to maintain some of the intermittency of heat fluxes within a winter. Notably, this experiment performs worse than the other two experiments, with a much lower correlation and higher RMSE. It has particular difficulty in simulating extreme years, both the weak convection in 09-10 and the strong convection in 14-15. These extreme years are more accurately simulated in Experiment 2 with constant stratification and variable forcing, suggesting that the variability in surface forcing is dominant.

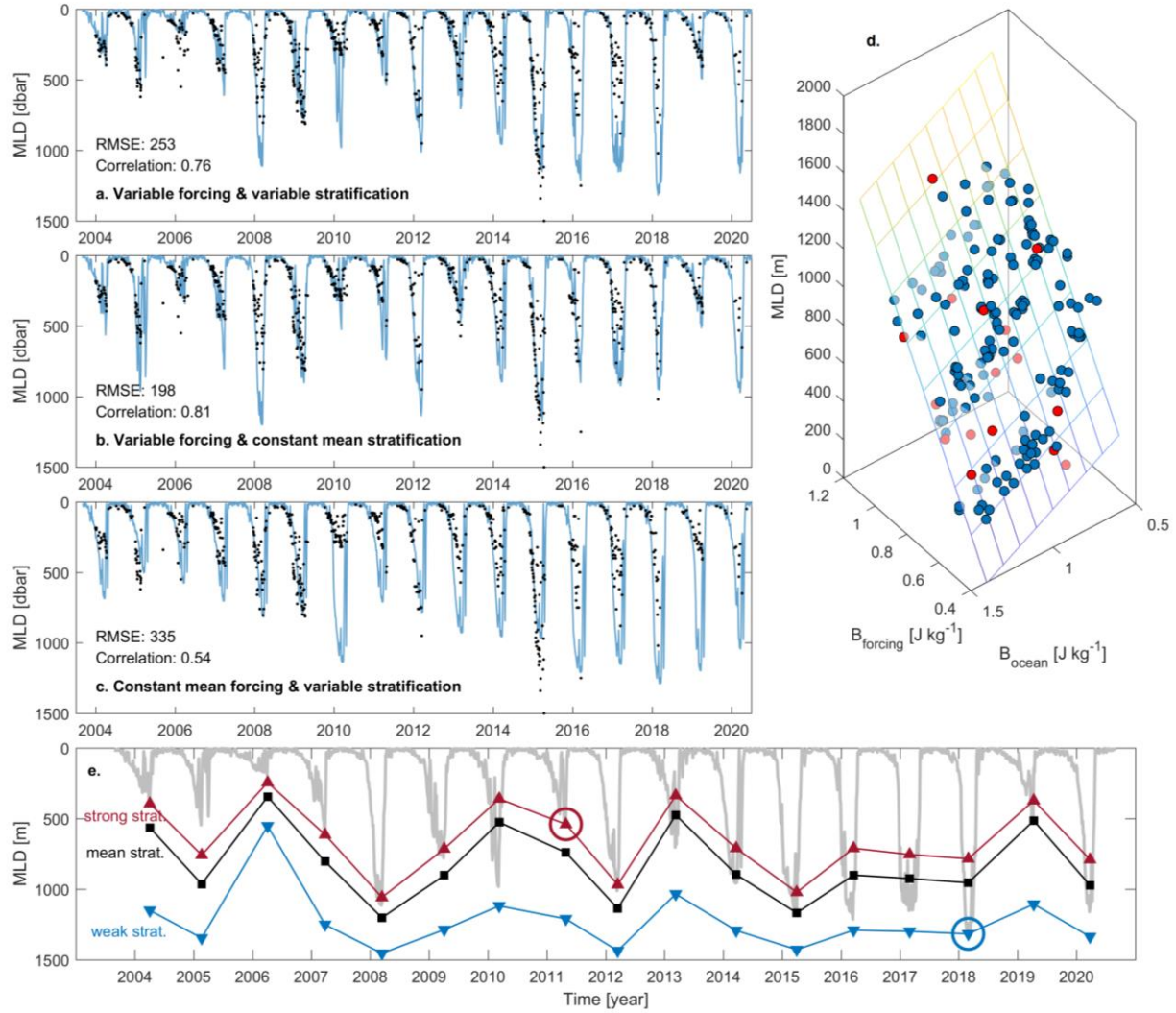


Figure 7. Results from the PWP experiments. Panels **a-c** show examples of the three types of PWP model experiments (in blue) compared to observed MLD (in black). **a.**) Reconstruction of observed variability in MLD with both varying forcing and stratification, **b.**) investigating role of forcing by applying the observed variable forcing and initializing using summer mean constant stratification, **c.**) investigating the role of stratification by applying the identical forcing each year and re-initializing annually with the observed summer stratification. The root mean square error (RMSE) and the correlation (significant at the 95% level) between simulated and observed MLD is noted in each panel. **d.**) 2D linear regression fit of annual maximum MLD on forcing and stratification over the upper 1000 m. PWP points used for fit in blue, observations in red. **e.**) Annual maximum MLD under different stratifications. Variable forcing is applied on a repeated stratification that is either strong (2010 summer condition, in red), average (in black), or weak (2017 summer conditions, in blue). Grey line in the background is the reconstruction of the full variability (as in panel a.).

In the PWP model, the annual maximum MLD is a good representation of the intensity of convection as it is strongly correlated ($R = 0.93$) to the mean of the 30 deepest MLD in a winter. Therefore, the annual maximum MLD is used in the following analysis.

Figure 7d shows annual maximum MLDs against forcing and stratification for all PWP runs done, comprising of a total of 187 winters. This allows us to disentangle the dependence of MLD

on both in more detail than the observation record allows. A multivariate (2D) linear regression of MLD on B_{forcing} and B_{ocean} yields a dependence on B_{forcing} that is about three times as large as that of B_{ocean} . While this linear approximation is very simplified and based on a model with simplified dynamics, it does fit the observations (in red in Fig. 7d and not used for the fit) quite well. While the role of forcing is stronger, it is still interesting to quantify the impact of stratification in the context of climate change trends and the projected increase in stratification in the future. PWP Experiment 2 allows us to compare differences in maximum annual MLDs for model runs initialized with weakly versus average or strongly stratified water column and subjected to 19 different atmospheric forcings (Fig. 7e). First of all, in the case of the weakest stratification (using conditions for summer 2017) the mixed layer is substantially deeper than in the average stratification case. Notably, the values of the average stratification of all years lies within 1% of the midwaypoint between that of the minimum and maximum stratification. The mean MLD over all years in the weakly stratified case is 1230 ± 211 m, versus 823 ± 257 m in the average stratification case. In the weakly stratified case, The MLDs of the winters after 2007 are very similar in depth and we suspect that it is the deep stratification related to the transition from convective waters to the overflow waters beneath contribute as a limiting factor to MLD here. In the strong stratification case (using conditions of summer 2010) the mean MLD over all years is 655 ± 248 m, which is a shallowing of the mean by about 170 m. The additional stratification in 2010 was related to a very warm and fresh uppermost layer. Once this layer is removed, the stratification of the remaining profile is more similar to other years and the variability in MLDs between years is similar to that of the average stratification case. This means that even with this strong stratification, MLDs of 1200 m may still be reached in occasional strong winters (Fig. 7e).

4 Discussion and conclusions

We have presented here a novel weekly 19-year time series of hydrography and convection in the central Irminger Sea (Fig 4) based on mooring and Argo float data collected from 2002-2020. Using a 70-year annual time series (Fig 2), we have demonstrated that the variability in the hydrography, stratification, and atmospheric forcing during mooring period is comparable to the longer term variability. These time series data enable us to interpret recent Irminger Sea observations in the context of large variability previously identified on decadal time scales (van Aken et al., 2011; Josey et al., 2018; Chafik et al., 2022). Van Aken et al. (2011), describing the record up to 2010, identified six events with low PV and high dissolved oxygen concentrations at 1500 dbar, a typical signature of convectively ventilated water masses. The strongest of these was the event that occurred in the early 1990s, which produced a particularly cold, fresh and dense water mass. In the extended record, this event still stands out (Figure 2). The more recent low PV event, initiated with the strong convection in the winter of 2014-2015, rivals that of the 1990s in term of low PV, but is less dense and therefore shallower.

The 19-year mooring record gives insight into the range of interannual variability in convection, with MLD reaching only 288 dbar in 09-10 and down to 1500 dbar in 14-15. Mixed layers shallower than 500 dbar do not leave an imprint on the local PV profile, as this layer is completely restratified, but deeper mixed layers do. Both the observations and simulations with the PWP MLD model indicate that the depth of convection is determined mainly by the strength of the atmospheric buoyancy forcing in winter, with a maximum around 1500 dbar because of an

increased deep density gradient associated with the transition to overflow waters. Winters with very shallow convection after strong stratification (03-04, 09-10 and 18-19) coincided with weaker than average atmospheric forcing. This result agrees with findings of Kim et al. (2021), who posited that weak convection during a GSA in the Labrador Sea was also mainly caused by weak atmospheric forcing. However, the fresh anomaly arriving in the Irminger Sea towards the end of the mooring record (de Jong et al., 2020; Holliday et al., 2020; Bilo et al., 2022) does have an effect on the hydrography, as these fresh waters are mixed into the water column and freshened the waters at intermediate depths. Despite the lower salinities, the cold character of the strong convection from 2014 to 2018 created a class of mid-depth waters in the Irminger Sea that is the densest in the 19-year record.

The timing of the return of convection in the winter of 14-15 is auspicious, as this was also the first winter observed by the OSNAP array and the OOI moorings. However, the sudden transition from a warm, buoyant and high ADT period to a period of cold, dense and low ADT preceded the addition of these new observations. This makes the long-term context provided by the new 2002-2020 weekly time-series presented here especially critical to contextualize analyses of OSNAP and OOI data. Since convection has weakened after 2018, it is likely that the Irminger Sea will return to a warm, buoyant period, but this restratification is much more gradual. The overturning at OSNAP East is related to water mass transformation of all buoyant waters to waters denser than 27.53 kg m^{-3} (Lozier et al., 2019; Li et al., 2021; Petit et al., 2020). The convection at the mooring locations in the central Irminger Sea adds mainly to the densest waters formed, however the atmospheric forcing driving the variability at this locations is coherent over a much wider area. Mixing along the boundaries (Le Bras et al., 2020, Le Bras et al. 2022) as well as shallower mixing over more stratified waters further east (de Jong et al., 2020) will contribute to the total overturning as well, but will likely follow the same interannual variability. The weak stratification in the cyclonic Irminger Gyre and the position underneath the strong atmospheric forcing by the Greenland Tip Jet acts to exacerbate the interannual variability in the resulting MLD. This is reflected in the minimum in ADT identified as a center of action for the Subpolar Gyre by Chafik et al. (2022), which we here find is related mainly to local convection and not to the advection of intermediate waters from elsewhere. Continued measurements in the central Irminger Sea will be essential to understanding overturning in the Subpolar Gyre.

We showed that in the past 19 years of the Irminger Sea, and likely the last 70, stratification and forcing are in a part of parameter space such that strong forcing will always penetrate the initial stratification of the upper layer, so the stratification matters little as long as strong forcing persists. Once the stratification over the upper layer is removed the mid-depth layer is relatively easy to homogenize until the transition to overflow derived waters at 1500 m is reached. Additionally, we found that the maximum stratification in summer relies strongly on convection in the previous winter. This agrees with the finding of Sterl & de Jong (2022) that there is little interannual variability in the strength of restratification over the upper 600 m in the Irminger Sea. This gives the atmospheric forcing additional importance as it sets both the strength of convection in the current year as well as the next. Under climate change, the stratification of the Irminger Sea is projected to strengthen as a result of a warming upper ocean and an increase in freshwater input. Conditions such as in 2010 and 2019 will become more prevalent, moving the Irminger Sea to the edge of the currently observed parameter space in terms of stratification.

Under those conditions, convection could shallow by 170 m on average. but deep MLDs of up to 1200 m could still occur under strong forcing (Fig. 7e). In those cases stratification would be significantly reduced for the subsequent years, possibly allowing deep convection to return again under somewhat weaker forcing (similar to 08-09 in Fig. 5 and de Jong et al. 2012). However, once the stratification moves outside the current parameter space, it's impact may be larger with our results suggesting that the thickness of the layer over which the additional buoyancy is spread determining the impact on MLD. Nevertheless, future forcing conditions are likely to change as well as may have a larger impact on MLD while we are still in the current parameter space. For example, less frequent occurrences of Tip Jets due to a shift in the Jet Stream or a warmer atmosphere and reduced air-sea temperature difference could significantly reduce heat loss and thereby weaken MLD more substantially than an increase in stratification. Therefore, changes in atmospheric forcing may need to be taken into account when considering changes in convection.

Acknowledgments

MFdJ is financially supported by the Innovational Research Incentives Scheme of the Netherlands Organisation for Scientific Research (NWO) under grant agreement nos. 016.Vidi.189.130. KEF and HIP were supported by the US National Science Foundation (NSF) under award #1946072. ILB was supported by the NSF under awards OCE-2038481 and OCE-2122579.

The Long-term Ocean-Climate Observations (LOCO) program was started in 2003 as a NWO-financed large investment programme (NWO Groot), of which the central Irminger Sea mooring was one component. This particular LOCO mooring was continued as part of the European Community's 7th framework programme (FP7/2007–2013) under grant agreement No. GA212643 (THOR: "Thermohaline Overturning – at Risk", 2008–2012), European Union 7th Framework Programme (FP7 2007–2013) under grant agreement n.308299 NACLIM in 2012 and finally under the Horizon 2020 Research and Innovation Program under Grant 727852 (Blue-Action) in 2016. Occasional gaps between funding sources were covered by the Royal Netherlands Institute for Sea Research (NIOZ).

The CIS Mooring received funding by the EU FP5 ANIMATE (EVR1-CT-2001-40014), EU FP6 MERSEA (502885), EU FP7 EuroSITES (202955), EU FP7 FixO3 (312463), EU FP7 NACLIM (308299), BMBF Nordatlantik, BMBF RACE, Deutsche Forschungsgemeinschaft within the METEOR/MERIAN core program.

Ocean Observatories Initiative (OOI) is a major facility fully funded by the National Science Foundation under Cooperative Agreement No. 1743430, and the Woods Hole Oceanographic Institution OOI Program Office.

Argo data were collected and made freely available by the International Argo Program and the national programs that contribute to it (<https://argo.ucsd.edu>, <https://www.ocean-ops.org>). The Argo Program is part of the Global Ocean Observing System. The authors thank the many research vessels and crews that have contributed to the collection of these data over the last 70 years.

Open Research

Data from LOCO deployments between 2003 and 2011 are available from the OceanSITES repository at https://www.ndbc.noaa.gov/data/oceansites/deployment_data/LOCO-IRMINGSEA/. Data from LOCO deployments between 2012 and 2018 are available through the following DOIs:

- de Jong, Marieke Femke (2023). Hydrography and velocity data from the Long-term Ocean Circulation Observations (LOCO) mooring in the central Irminger Sea: Deployment nine (LOCO2_9) July 2011 to August 2012, <https://doi.org/10.25850/nioz/7b.b.mg>, NIOZ, V1

- de Jong, Marieke Femke (2023). Hydrography and velocity data from the Long-term Ocean Circulation Observations (LOCO) mooring in the central Irminger Sea: Deployment ten (LOCO2_10) August 2012 to July 2014, <https://doi.org/10.25850/nioz/7b.b.ng>, NIOZ, V1

- de Jong, Marieke Femke (2023). Hydrography and velocity data from the Long-term Ocean Circulation Observations (LOCO) mooring in the central Irminger Sea: Deployment eleven (LOCO2_11) September 2014 to July 2015, <https://doi.org/10.25850/nioz/7b.b.pg>, NIOZ, V1

- de Jong, Marieke Femke (2023). Hydrography and velocity data from the Long-term Ocean Circulation Observations (LOCO) mooring in the central Irminger Sea: Deployment twelve (LOCO2_12) July 2015 to August 2016, <https://doi.org/10.25850/nioz/7b.b.qg>, NIOZ, V1

de Jong, Marieke Femke (2023). Hydrography and velocity data from the Long-term Ocean Circulation Observations (LOCO) mooring in the central Irminger Sea: Deployment thirteen (LOCO2_13) August 2016 to June 2018, <https://doi.org/10.25850/nioz/7b.b.rg>, NIOZ, V1

Quality controlled OOI profile data used in this study is available through:
Le Bras, Isabela (2023). Potential temperature and salinity profiles from the Ocean
Observatories Initiative Global Irminger Sea Array Apex profiler mooring from September 2014
to May 2020 (NCEI Accession 0285241). NOAA National Centers for Environmental
Information. Dataset. <https://www.ncei.noaa.gov/archive/accession/0285241>.

References

Belkin, I. M., S. Levitus, J. I. Antonov, & Malmberg, S.-A. (1998), “Great Salinity Anomalies”
in the North Atlantic. *Progress in Oceanography*, 41, 1– 68. [https://doi.org/10.1016/S0079-6611\(98\)00015-9](https://doi.org/10.1016/S0079-6611(98)00015-9)

Biló, T. C., Straneo, F., Holte, J., & Le Bras, I. A.-A. (2022), Arrival of new Great Salinity
Anomaly weakens convection in the Irminger Sea. *Geophysical Research Letters*, 49,
e2022GL098857. <https://doi.org/10.1029/2022GL098857>

Böning, C. W., Scheinert, M., Dengg, J., Biastoch, A., & Funk, A. (2006). Decadal variability of
subpolar gyre transport and its reverberation in the North Atlantic overturning, *Geophysical
Research Letters*, 33, L21S01, doi:10.1029/2006GL026906.

Böning, C. W., Behrens, E., Biastoch, A., Getzlaff, K. & Bamber, J. L. (2016), Emerging
impact of Greenland meltwater on deepwater formation in the North Atlantic
Ocean. *Nature Geoscience*, 9, 523–527. <https://doi.org/10.1038/ngeo2740>

Chafik, L.; Holliday, N. P. ; Bacon, S., & Rossby, T. (2022), Irminger Sea is the center of action for subpolar AMOC variability. *Geophysical Research Letters*, 49 (17).

<https://doi.org/10.1029/2022GL099133>

de Jong, M. F., van Aken, H. M., Våge, K. & Pickart, R. S. (2012), Convective mixing in the central Irminger Sea: 2002–2010. *Deep Sea Research I*, 63, 36–51.

<https://doi.org/10.1016/j.dsr.2012.01.003>

de Jong, M. F., & de Steur, L. (2016), Strong winter cooling over the Irminger Sea in winter 2014–2015, exceptional deep convection, and the emergence of anomalously low SST.

Geophysical Research Letters, 43 (13), 7106–7113. <https://doi.org/10.1002/2016GL069596>

de Jong, M. F., Olmanns, M., Karstensen, J., & de Steur, L. (2018), Deep convection in the Irminger Sea observed with a dense mooring array. *Oceanography*, 31(1), 50–59.

<https://doi.org/10.5670/oceanog.2018.109>

de Jong, M. F., Steur, L., Fried, N., Bol, R., & Kritsotakis, S. (2020), Year-round measurements of the Irminger current: Variability of a two-core current system observed in 2014–2016. *Journal of Geophysical Research: Oceans*, 125, e2020JC016193.

<https://doi.org/10.1029/2020JC016193>

Dickson, R. R., Meincke, J., Malmberg, S.-A., & Lee, A. J. (1988), The “great salinity anomaly” in the Northern North Atlantic 1968–1982. *Progress in Oceanography*, 20(2), 103-151.

[https://doi.org/10.1016/0079-6611\(88\)90049-3](https://doi.org/10.1016/0079-6611(88)90049-3)

Duyck, E., Gelderloos, R., & de Jong, M. F. (2022). Wind-driven freshwater export at Cape Farewell. *Journal of Geophysical Research: Oceans*, 127, e2021JC018309.

<https://doi.org/10.1029/2021JC018309>

Eden, C., & Willebrand, J. (2001). Mechanism of Interannual to decadal variability of the North Atlantic circulation. *Journal of Climate*, 14, 226-2280. [https://doi.org/10.1175/1520-0442\(2001\)014%3C2266:MOITDV%3E2.0.CO;2](https://doi.org/10.1175/1520-0442(2001)014%3C2266:MOITDV%3E2.0.CO;2)

Gelderloos, R., Straneo, F., & Katsman, C. A. (2012), Mechanisms behind the Temporary Shutdown of Deep Convection in the Labrador Sea: Lessons from the Great Salinity Anomaly Years 1968–71. *Journal of Climate*, 25(19), 6743-6755.

<https://journals.ametsoc.org/view/journals/clim/25/19/jcli-d-11-00549.1.xml>

Hersbach, H., Bell, B., Berrisford, P., Biavati, G., Horányi, A., Muñoz Sabater, J., Nicolas, J., Peubey, C., Radu, R., Rozum, I., Schepers, D., Simmons, A., Soci, C., Dee, D., & Thépaut, J.-N. (2018), ERA5 hourly data on single levels from 1959 to present. Copernicus Climate Change Service (C3S) Climate Data Store (CDS). (Accessed on 14-APR-2021), 10.24381/cds.adbb2d47

Holliday, P. N., Bersch, M., Berx, B., Chafik, L., Cunningham, S., Florindo-López, C., Hátún, H., Johns, W., Josey, S. A., Larsen, K. M. H., Mulet, S., Olthmanns, M., Reverdin, G., Rossby, T.,

Thierry, V., Valdimarsson, H., & Yashayaev, I., (2020), Ocean circulation causes the largest freshening event for 120 years in eastern Subpolar North Atlantic. *Nature Communications*, 11(1), 585. <https://doi.org/10.1038/s41467-020-14474-y>

Holte, J., & Straneo, F. (2017), Seasonal overturning of the Labrador Sea as observed by Argo floats. *Journal of Physical Oceanography*, 47(10), 2531–2543. <https://doi.org/10.1175/JPO-D-17-0051.1>

Josey, S. A., de Jong, M. F., Olthmanns, M., Moore, G. K., & Weller, R. A. (2019), Extreme variability in Irminger Sea winter heat loss revealed by Ocean Observatories Initiative mooring and the ERA5. Reanalysis. *Geophysical Research Letters*, 46, 293–302. <https://doi.org/10.1029/2018GL080956>

Katsman, C. A., Drijfhout, S. S., Dijkstra, H. A., & Spall, M. A. (2018), Sinking of dense North Atlantic waters in a global ocean model: Location and controls. *Journal of Geophysical Research: Oceans*, 123, 3563–3576. <https://doi.org/10.1029/2017JC013329>

Kim, W. M., Yeager, S., & Danabasoglu, G. (2021), Revisiting the causal connection between the Great Salinity Anomaly of the 1970s and the shutdown of Labrador Sea deep convection. *Journal Of Climate*, 34, 675–696. <https://doi.org/10.1175/JCLI-D-20-0327.1>

- 864 Lazarevich, P., Rossby, T., & McNeil, C. (2004), Oxygen variability in the near-surface waters
865 of the northern North Atlantic: Observations and a model. *Journal of Marine Research*, 62(5),
866 663–683. <https://doi.org/10.1357/0022240042387547>
867
- 868 Lazier, J. R. N. (1980), Oceanographic conditions at Ocean Weather Ship Bravo, 1964–1974.
869 *Atmosphere-Ocean Volume*, 18(3), 227-238. <https://doi.org/10.1080/07055900.1980.9649089>
870
- 871 Le Bras, I. A.-A., Straneo, F., Holte, J., de Jong, M. F., & Holliday, N. P. (2020), Rapid export of
872 waters formed by convection near the Irminger Sea's western boundary. *Geophysical Research*
873 *Letters*, 47, e2019GL085989. <https://doi.org/10.1029/2019GL085989>
874
- 875 Jerlov, N. G. (1968), Optical oceanography, Elsevier (1968), p. 194
876
- 877 Li, F., Lozier, M. S., Bacon, S., Bower, A. S., Cunningham, S. A., de Jong, M. F., deYoung, B.,
878 Fraser, N., Fried, N., Han, G., Holliday, N. P., Holte, J., Houpert, L., Inall, M. E., Johns, W. E.,
879 Jones, S., Johnson, C., Karstensen, J., Le Bras, I. A., Lherminier, P., Lin, X., Mercier, H.,
880 Olmanns, M., Pacini, A., Petit, T., Pickart, R. S., Rayner, D., Straneo, F., Thierry, V., Visbeck,
881 M., Yashayaev, I., & Zhou, C. (2021), Subpolar North Atlantic western boundary density
882 anomalies and the Meridional Overturning Circulation. *Nature Communications*, 12, 3002.
883 <https://doi.org/10.1038/s41467-021-23350-2>
884
- 885 Lozier, M. S., Bacon, S., Bower, A. S., Cunningham, S. A., de Jong, M. F., de Steur, L.,
886 deYoung, B., Fischer, J., Gary, S. F., Greenan, B. J. W., Heimbach, P., Holliday, N. P., Houpert,

- L., Inall, M. E., Johnson, H. L., Johns, W. E., Karstensen, J., Li, F., Lin, X., Mackay, N.,
 Marshall, N. P., Mercier, H., Myers, P. G., Pickart, R. S., Pillar, H. R., Straneo, F., Thierry, V.,
 Williams, R. G., Wilson, C., Yang, J., Zhao, J., & Zika, J. D. (2017), Overturning in the Subpolar
 North Atlantic Program: A new international ocean observing system. *Bulletin of the American
 Meteorological Society*, 98(4), 737–752. <https://doi.org/10.1175/BAMS-D-16-0057.1>
- Lozier, S. M., Li, F., Bacon, S., Bahr, F., Bower, A. S., Cunningham, S. A., de Jong, M. F., de
 Steur, L., deYoung, B., Fischer, J., Gary, S. F., Greenan, B. J. W., Holliday, N. P., Houk, A.,
 Houpert, L., Inall, M. E., Johns, W. E., Johnson, H. L., Johnson, C., Karstensen, J., Koman, G.,
 Le Bras, I. A., Lin, X., Mackay, N., Marshall, D. P., Mercier, H., Oltmanns, M., Pickart, R. S.,
 Ramsey, A. L., Rayner, D., Straneo, F., Thierry, V., Torres, D. J., Williams, R. G., Wilson, C.,
 Yang, J., Yashayaev, I., & Zhao, J. (2019), A sea change in our view of Overturning in the
 Subpolar North Atlantic. *Science*, 363, 516–521. <https://doi.org/10.1126/science.aau6592>
- Marshall, J., & Schott, F. (1999), Open ocean deep convection: Observations, models and theory.
Reviews of Geophysics, 37, 1– 64. <https://doi.org/10.1029/98RG02739>
- Moore, G. W. K. (2003), Gale force winds over the Irminger Sea to the east of Cape Farewell,
 Greenland. *Geophysical Research Letters*, 30, 1894. <https://doi.org/10.1029/2003GL018012>.
- Moore, G. W. K., & Renfrew, I. A. (2005), Tip jets and barrier winds: A QuickSCAT
 climatology of high wind speed events around Greenland. *Journal of Climate*, 18, 3713–3725.
<https://doi.org/10.1175/JCLI3455.1>.

910

911 Mulet, S., Rio, M.-H., Mignot, A., Guinehut S. & Morrow, R., (2012). A new estimate of the
912 global 3D geostrophic ocean circulation based on satellite data and in-situ measurements. *Deep*
913 *Sea Research Part II*, 77–80(0):70–81. <https://doi.org/10.1016/j.dsr2.2012.04.012>

914

915 Nansen, F. (1912), Das Bodenwasser und die Abkühlung des Meeres. *Internationale Revue der*
916 *gesamten Hydrobiologie und Hydrographie*, 5, 1–42. <https://doi.org/10.1002/iroh.19120050102>

917

918 Oltmanns, M., Karstensen, J., & Fischer, J. (2018), Increased risk of a shutdown of ocean
919 convection posed by warm North Atlantic summers. *Nature Climate Change*, 8(4), 300-304.
920 <https://doi.org/10.1038/s41558-018-0105-1>

921

922 Paulson, C. A., & Simpson, J. J. (1977), Irradiance Measurements in the Upper Ocean. *Journal*
923 *of Physical Oceanography*, 7(6), 952-956. [https://doi.org/10.1175/1520-](https://doi.org/10.1175/1520-0485(1977)007<0952:IMITUO>2.0.CO;2)
924 [0485\(1977\)007<0952:IMITUO>2.0.CO;2](https://doi.org/10.1175/1520-0485(1977)007<0952:IMITUO>2.0.CO;2)

925

926 Pickart, R. S., Straneo, F., & Moore, G. W. K. (2003), Is Labrador Sea Water formed in the
927 Irminger Basin? *Deep Sea Research I*, 50(1), 23–52. [https://doi.org/10.1016/S0967-](https://doi.org/10.1016/S0967-0637(02)00134-6)
928 [0637\(02\)00134-6](https://doi.org/10.1016/S0967-0637(02)00134-6)

929

930 Piron, A., Thierry, V., Mercier, H., & Caniaux, G. (2015), Observations of basin scale deep
931 convection in the Irminger Sea with Argo floats in the winter of 2011-2012. *Deep-Sea Research*
932 *I*, 109, 76–90. <https://doi.org/10.1016/j.dsr.2015.12.012>

933

934 Piron, A., Thierry, V., Mercier, H., & Caniaux, G. (2017), Gyre-scale deep convection in the
935 subpolar North Atlantic Ocean during winter 2014–2015. *Geophysical Research Letters*, 44,
936 1439–1447. <https://doi.org/10.1002/2016GL071895>

937

938 Petit, T., Lozier, M. S., Josey, S. A., & Cunningham, S. A. (2020), Atlantic deep water formation
939 occurs primarily in the Iceland Basin and Irminger Sea by local buoyancy forcing. *Geophysical*
940 *Research Letters*, 47, e2020GL091028. <https://doi.org/10.1029/2020GL091028>

941

942 Price, J. F., Weller, R. A., & Pinkel, R. (1986), Diurnal cycling: Observations and models of the
943 upper ocean response to diurnal heating, cooling, and wind mixing. *Journal of Geophysical*
944 *Research*, 91(C7), 8411–8427. <https://doi.org/10.1029/JC091iC07p08411>

945

946 Schmidt, S., & Send, U. (2007), Origin and composition of seasonal Labrador Sea freshwater.
947 *Journal of Physical Oceanography*, 37(6), 1445–1454. <https://doi.org/10.1175/JPO3065.1>

948

949 Sterl, M. F., & de Jong, M. F. (2022), Restratification structure and processes in the Irminger
950 Sea. *Journal of Geophysical Research: Oceans*, 127(12), e2022JC019126.
951 <https://dx.doi.org/10.1029/2022jc019126>

952

953 Straneo, F. (2006), On the connection between dense water formation, overturning, and poleward
954 heat transport in a convective basin. *Journal of Physical Oceanography*, 36, 1822– 1840.
955 <https://doi.org/10.1175/JPO2932.1>

- Sverdrup, H. U., Johnson, M. W., & Fleming, R. H. (1942), *The Oceans: Their Physics, Chemistry, and General Biology*. Prentice-Hall Inc., Englewood Cliffs, NJ, USA, 1,060 pp.
- van Aken, H. M., de Jong, M. F., & Yashayaev, I. (2011), Decadal and multi-decadal variability of Labrador Sea water in the north-western North Atlantic Ocean derived from tracer distributions: Heat budget, ventilation, and advection. *Deep-Sea Research I*, 58, 505–523. <https://doi.org/10.1016/j.dsr.2011.02.008>
- Woods, R. A., Keen, A. B., Mitchell, J. F., & Gregory, J. M. (1999). Changing spatial structure of the thermohaline circulation in response to atmospheric CO₂ forcing in a climate model. *Nature*, 399(6736), 572–575. <https://doi.org/10.1038/21170>
- Yashayaev, I. (2007), Hydrographic changes in the Labrador Sea, 1960–2005. *Progress in Oceanography*, 73, 242–276. <https://doi.org/10.1016/j.pocean.2007.04.015>
- Zhang, R., Sutton, R. Danabasoglu, G., Kwon, Y.-O., Marsh, R., Yeager, S. G. , Amrhein, D. E., and Little, C. M. (2019). A review of the role of the Atlantic meridional overturning circulation in Atlantic multidecadal variability and associated climate impacts. *Reviews of Geophysics*, 57, 316–375. <https://doi.org/10.1029/2019RG000644>